Chemical Engineering Journal 165 (2010) 482–489

Contents lists available at ScienceDirect

Chemical Engineering Journal

journal homepage: www.elsevier.com/locate/cej

Mixture design optimization of the composition of S, C, SnO_2-codoped TiO_2 for degradation of phenol under visible light

Lung-Chuan Chen[a,*], Chao-Ming Huang[b], Ming-Chieh Hsiao[b], Fu-Ren Tsai[c]

[a] Department of Polymer Materials, Kun-Shan University, Yung Kang City, Tainan 71003, Taiwan, ROC
[b] Department of Environmental Engineering, Kun-Shan University, Yung Kang City, Tainan 71003, Taiwan, ROC
[c] Department of electro-optical engineering, Kun-Shan University, Yung Kang City, Taiwan 71003, Taiwan, ROC

ARTICLE INFO

Article history:
Received 31 March 2010
Received in revised form 8 September 2010
Accepted 10 September 2010

Keywords:
Mixture design
Response surface
Photocatalysis
Sulfur
Tin oxide

ABSTRACT

We have applied mixture design and response surface techniques to prepare visible light-active TiO_2 photocatalysts codoped with sulfur, carbon, and tin oxide using titanium tetraisopropoxide (TTIP), tin(IV) chloride, and thiourea, respectively, as precursors. During calcination, the S atoms replaced the Ti or O atoms in the TiO_2 structure to maintain the anatase form, whereas doping with SnO_2 promoted the anatase-to-rutile transformation. O–Ti–C bonds and carbonaceous species were present in the prepared samples; together with the S atoms, they were responsible for the visible light activity, which was boosted by moderate doping SnO_2 due to a declined e^-–h^+ recombination rate. A synergic effect induced by dopants SnO_2 and S, C on the visible light activity of TiO_2 was quantitatively established for the first time through mixture design techniques and response surface methodologies. The obtained empirically quartic models describe well the main and interactive influences of the precursors on the specific surface area and visible light activity of the S, C, SnO_2-codoped TiO_2 samples.

1. Introduction

Photocatalysis has attracted considerable interests on applications in environmental systems. The complete mineralization – to carbon dioxide and inorganic constituents – of contaminants in liquid and gas phases through photocatalysis at room temperature is a potential alternative to such currently used methods as chlorination, ozonation, and adsorption on active carbon [1–3]. TiO_2 is by far the most widely employed photocatalytic semiconducting material because of its chemical inertness, photostability, low cost, and nontoxicity. Although much effort has been devoted to improving its photocatalytic activity, TiO_2 exhibits low efficiency under visible light because it has a large band gap energy of 3.2 eV, corresponding to a threshold wavelength of 388 nm.

Nonmetallic elements doping has been regarded as a promising strategy for improving visible light activity of TiO_2-based photocatalysts [3,4]. Among such techniques, carbon, sulfur, and nitrogen atoms have been shown to effectively enhance visible light activity of TiO_2. These nonmetallic atoms can substitute for the lattice Ti^{4+} and/or O^{2-} species in the TiO_2 structure with the corresponding cationic and anionic forms, respectively, causing substantial improvements in visible light activity as compared to that of pure TiO_2 due to band gap narrowing by the mixing of energy levels of electrons of nonmetallic elements and O atoms, or introduction of new energy levels within the band gap of TiO_2 [4–18]. Although these reports indicate that doping with nonmetallic elements is an efficient approach toward increase the photocatalytic activity of TiO_2 under visible light, the photocatalytic activity remains low and must be improved further if such materials are to find commercial applications.

One of the main drawbacks leading to low photocatalytic activity is recombination of photogenerated electrons and holes. Reducing this recombination process is considered as an effective route to significantly increase the activity. The combination of two semiconductors having their conduction and valence bands at different energy levels is one approach toward improving photocatalytic activity by increasing the charge separation efficiency, charge carrier lifetime, and interfacial charge transfer rate [3]. The energy levels of the valence and conduction bands of TiO_2 are 2.7 and −0.5 V, respectively; for SnO_2, they are 3.7 and 0.0 V, respectively (versus NHE) [3,19,20]. Therefore, upon photoexcitation of a TiO_2/SnO_2 composite, a photoelectron generated on TiO_2 will be injected into the conduction band of SnO_2, while the hole remains on TiO_2. Furthermore, the fact that the conductivity of SnO_2 is superior to that of TiO_2 also benefits the separation of photogenerated charged carriers.

Based on these findings, TiO_2 samples doped simultaneously with nonmetal species and SnO_2 are anticipated to apparently enhance photocatalytic activities under visible light; to date, however, the photocatalytic activity of S, C, and SnO_2-codoped TiO_2

* Corresponding author. Tel.: +886 6 2059427; fax: +886 6 2059422.
E-mail address: lcchen@mail.ksu.edu.tw (L.-C. Chen).

1385-8947/$ – see front matter © 2010 Elsevier B.V. All rights reserved.
doi:10.1016/j.cej.2010.09.044

samples has not been reported. It should be noted that the composition of the codoped TiO_2 photocatalyst can affect their photocatalytic activities to a great extent; however, no systematic study about the composition effect has been conducted. When using traditional methods, it is difficult to determine the combined influences of each of the components in the composite on the photoactivity, particularly the interaction effect between the components. Statistical strategies can provide facile and effective approaches to establish the quantitative relationship between dependent and independent variables [21–25]. Hence, in this study we used a mixture design technique and a response surface method to elucidate the effect of the composition of the precursors on the specific surface area and visible light activity of TiO_2 in terms of its ability to mediate the photodegradation of phenol. We have firstly and successfully obtained a quantitative equation describing the influence of the compositions of the precursors on the photocatalytic activity and specific surface area. Furthermore, properties of the prepared S, C, and SnO_2-codoped TiO_2 were characterized and correlated well with the photocatalytic activity.

2. Experimental

2.1. Catalyst preparation

Doped TiO_2 samples were prepared according to procedures described previously with little modification [9]. Typically, 0.10 mole TTIP (Acros, 97%) was added into 200 mL anhydrous ethanol under mild stirring, and then 0.025 mole $SnCl_4$ (Showa, EP) and 0.025 mole thiourea (Wako, EP) were added in sequence to prepare the sample with mole fractions of TTIP, $SnCl_4$, and thiourea of 0.66, 0.17, 0.17. The resulting solution was further stirred for 2 h. After then, the solution was concentrated to obtain a white slurry product by evaporating ethanol under reduced pressure. This slurry product was aged for 2 days at room temperature to form a powder sample, which was further dried in an oven at 60 °C for 12 h, followed by calcination at 400 °C for 3 h with a risen rate of 3 °C/min. The obtained samples were grounded and washed with distillated water for three times. Undoped TiO_2 samples were also prepared using a similar procedure (i.e., without the addition of $SnCl_4$ and thiourea). The symbols P, T, U, and TU represent the pristine, $SnCl_4$-, thiourea-, and $SnCl_4$/thiourea-modified TiO_2 samples, respectively. According to the mixture design method, the mole fractions of the ingredients present summed to 1.0, an equilateral triangle can be applied to represent the compositions of the constituents in a tertiary system, with vertexes corresponding to the pure components and the points on and inside the boundaries representing the simultaneous occurrence of two and three components, respectively, in a system with no upper or lower limitations of each component. Note, however, that in this study we restricted the mole fraction of TTIP to no less than 0.5 because TiO_2 was the main constituent responsible for the photocatalytic activity. Therefore, we established a new equilateral triangle by transforming the actual composition to the pseudo-composition, according to the equation $Z_i = (X_i - L_i)/R$, where Z_i is the pseudo-composition of component i, L_i is the lower limit of the composition for X_i, and $R = 1 - \Sigma L_i$ [24,25]. Hereafter, suffixes of 1, 2, and 3 in X_i and Z_i represent TTIP, $SnCl_4$, and thiourea, respectively. Table 1 lists the designed compositions for the mixture experiments.

2.2. Characterization

The crystal phases of the prepared samples were identified through X-ray diffraction (XRD) using a Siemens D5000 X-ray diffractometer. A Raman spectrometer (Ventuno, Jasco) was also employed to identify the structure of the prepared samples. Fourier transform infrared (FTIR) spectra were recorded using a Bio-Rad Digilab FTS-40 instrument. Optical absorption spectra of the samples were obtained using a UV–vis spectrophotometer equipped with an integrated sphere assembly (Jasco, V-550). X-ray photoelectron spectroscopy (XPS) was performed using an ESCA PHI 5000 instrument and Al Kα irradiation (1486.6 eV) to determine the chemical states of Ti, S, O, and C atoms in the prepared samples. The specific surface areas, pore volumes, and pore sizes of the powder samples were measured using Barrett–Emmett–Teller (BET) and Barrett–Joyner–Halenda (BJH) techniques on a Micromeritics ASAP 2020 apparatus.

Table 1
Actual and pseudo compositions of the prepared samples for the mixture design.

Samples	Actual composition			Pseudo composition		
	TTIP X_1	$SnCl_4$ X_2	Thiourea X_3	TTIP Z_1	$SnCl_4$ Z_2	Thiourea Z_3
TU-01	0.58	0.33	0.083	0.17	0.67	0.17
TU-02	0.58	0.083	0.33	0.17	0.17	0.67
TU-03	0.67	0.17	0.17	0.33	0.33	0.33
U-04	0.83	0	0.17	0.67	0	0.33
TU-05	0.67	0.17	0.17	0.33	0.33	0.33
T-06	0.83	0.17	0	0.67	0.33	0
P-07	1	0	0	1	0	0
TU-08	0.83	0.083	0.083	0.67	0.17	0.17
TU-09	0.67	0.17	0.17	0.33	0.33	0.33
U-10	0.5	0	0.5	0	0	1
TU-11	0.71	0.083	0.21	0.42	0.17	0.42
T-12	0.5	0.5	0	0	1	0
TU-13	0.67	0.17	0.17	0.33	0.33	0.33
TU-14	0.5	0.17	0.33	0	0.33	0.67
T-15	0.67	0.33	0	0.33	0.67	0
TU-16	0.58	0.21	0.21	0.17	0.42	0.42
TU-17	0.67	0.17	0.17	0.33	0.33	0.33
TU-18	0.71	0.21	0.083	0.42	0.17	0.17
TU-19	0.5	0.333	0.17	0	0.67	0.33
U-20	0.67	0	0.33	0.33	0	0.67

2.3. Photocatalytic activity

The photocatalytic activities of the doped and undoped TiO_2 samples were estimated by measuring the degradation of phenol in an aqueous solution under visible light. A cylindrical double-wall Pyrex reactor was used for photocatalytic measurements; isothermal water flowing in and out through the space between the walls controlled the reaction temperature at 25 °C. A Xe lamp (Oriel, 6271) operated at 900 W was used as the light source; its rays were passed through a 400 nm long pass filter (ZUL0400, Asahi Spectra Co.) to ensure that only visible light entered the reactor. At the beginning of each run, an aqueous suspension (250 mL) containing phenol (0.21 mM) and the photocatalyst (0.25 g) were fed into the reactor. Prior to illumination, the suspension was stirred in the dark for 60 min to achieve an equilibrium state. Samples were periodically taken from the reactor, centrifuged at 6000 rpm for 10 min, and then filtered through a 0.22-μm membrane filter prior to analysis using a Perkin-Elmer 200S high-performance liquid chromatography (HPLC) system equipped with a C18 column [1,26,27].

3. Results and discussion

Fig. 1 presents the XRD patterns of the P-, T-, U-, and TU-TiO_2 samples calcined at 400 and 600 °C. The 400 °C-calcined P-, U- and TU-TiO_2 samples revealed only the anatase phase of TiO_2; in contrast, the 400 °C-calcined T-TiO_2 sample featured predominantly the rutile phase. These results suggest that the presence of SnO_2 promoted the formation of the rutile phase as a result of similarity of cell parameters a and c between rutile TiO_2 and SnO_2

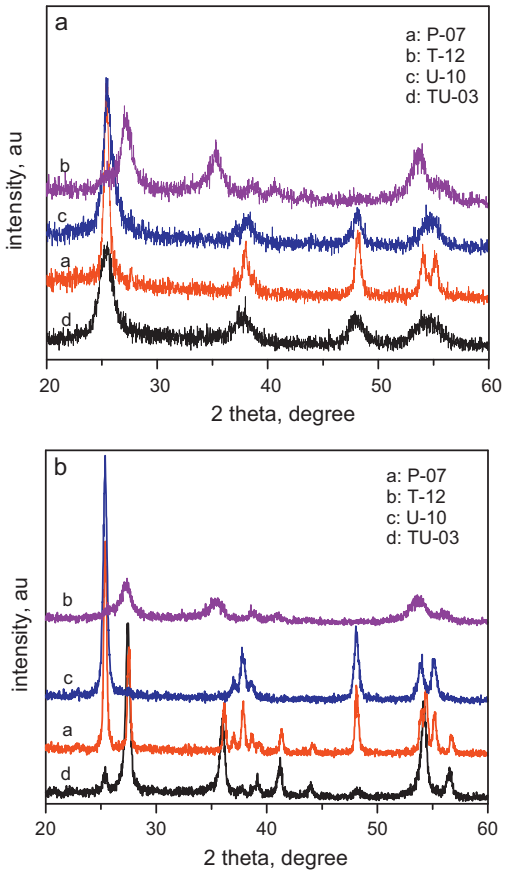

Fig. 1. XRD spectra of the P-07, T-12, U-10, and TU-03 samples calcined at (a) 400 and (b) 600 °C.

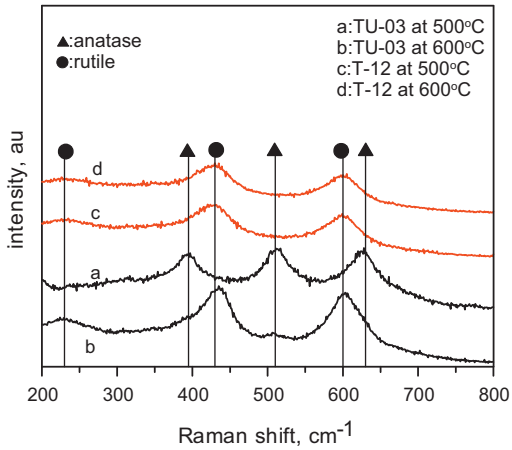

Fig. 2. Raman spectra of the T-12 and TU-03 samples calcined at 500 and 600 °C.

[28–30]. When we increased the calcination temperature to 600 °C, we observed ca. 36.5 and 91.0% of the rutile phase in the P- and TU-TiO_2 samples, respectively; in contrast, the U-TiO_2 sample still exhibited only an anatase phase, implying that addition of thiourea stabilized the anatase phase of TiO_2 [31–33] and raised the temperature for its anatase-to-rutile transition to above 600 °C, which is important to elevate photocatalytic activity of S, C, SnO_2-codoped TiO_2 because the anatase phase usually exhibits much higher photocatalytic efficiency than the rutile phase. Due to the insufficiency of water employed, the complete hydrolysis of TTIP is limited in this work. Instead, thiourea molecules can be chelated to TTIP through their nucleophilic ligands. Decomposition of thiourea during heat treatment causes the formation of S, C-doped TiO_2 and inhibits the crystallization of rutile TiO_2 at a lower temperature [31–34]. The main diffraction band of crystalline SnO_2 occurs at a value of $2\theta = 26.6°$ (1 1 0); it probably overlaps with the (1 0 1) and (1 1 0) crystalline planes of TiO_2 and, therefore, XRD techniques may not be appropriate for identifying SnO_2 crystallinity. As a result, we used Raman spectroscopy to examine whether or not crystalline SnO_2 existed in the samples. Fig. 2 presents the Raman spectra of T- and TU-TiO_2 samples prepared at 500 and 600 °C. Referring to the reported Raman bands of SnO_2 [35], we concluded that the formation of crystalline SnO_2 was insignificant because the main Raman bands of crystalline SnO_2 (at 776, 636, 574, and 490 cm^{-1}) were absent, presumably because of its lower abundance and greater difficulty in developing its crystal structure relative to that of TiO_2. The Raman spectra also indicated that the TU-TiO_2 samples exhibited the anatase-only phase when calcined at temperatures below 500 °C; the transformation to the rutile phase occurred when we increased the temperature to 600 °C, consistent with the XRD results. In addition, we cannot identify any peak attributed to SnS or SnS_2 component in the TU-TiO_2 sample from XRD and Raman patterns.

We applied XPS to determine the chemical states of the components in the TU-TiO_2 sample (TU-14) after using Ar^+ to etch away a 2 nm layer. Fig. 3a presents the XPS spectrum of the Ti 2p energy level of the sample. We attribute the two bands centered at 457.4 and 463.1 eV to the $2p_{3/2}$ and $2p_{1/2}$ spin–orbital splitting photoelectrons in Ti^{4+}. Furthermore, we used a curve fitting technique to identify two peaks at ca. 455.8 and 461.3 eV that originated from the Ti $2p_{3/2}$ and $2p_{1/2}$ electrons, respectively, of Ti^{3+} ions, revealing the presence of Ti^{3+} in addition to Ti^{4+} [36,37]. The binding energies of the $2p_{3/2}$ and $2p_{1/2}$ electrons in Ti^{4+} in this study are ca. 1.0 eV less than the reported values. Furthermore, three insignificant peaks centered at 454.2, 459.1, and 464.3 eV are also observed. We speculate that the presence of C and S atoms in the sample is the predominant cause for these observations.

Fig. 3b presents XPS spectra representing the chemical state of the C atoms in the TU-TiO_2 samples calcined at 400 and 600 °C. We attribute the band at 282.8 eV to the presence of O–Ti–C bonds [8], and the bands at 283.6 and 284.6 eV to the presence of carbonaceous and elemental carbons, and the bands at 287.0 and 287.6 eV to the presence of C–O and/or C=O bonds [8,36,38,39] for the sample calcined at 400 °C. It should be noted that adventitious carbons from the carbon tape used in the XPS measurement may also contribute to the XPS peak around 284.6 eV, therefore, its intensity should not be employed as the quantitative standard [15]. The results indicate that C atoms primarily substitute for O atoms in the TiO_2 structure, forming O–Ti–C bonds. In contrast, we found that substitution of Ti sites by C atoms was insignificant as indicated by that the area of the band belonging to the Ti–O–C units was relatively smaller than that of the O–Ti–C bonds, which was probably due to the large difference in the ionic radius between Ti^{4+} (0.068 nm) and C^{4+} (0.016 nm) [40]. When the calcined temperature increases from 400 to 600 °C, the distribution of carbon states exhibits apparent change. Most O–Ti–C bands disappear as a result of oxidation on calcination, particularly at a temperature higher than 400 °C [41]. On the other hand, a broad band around 285.0 eV sharply increases. Pillai et al. [33] and Shi et al. [42] have pointed out that carbon can occur as a solid solution within the interstices of anatase crystal above 500 °C and display a binding energy near 285 eV. Accordingly, the increase of this band may be ascribed to the formation of a solid solution in addition to carbonaceous species and elemental carbons. For comparison, the chemical state of carbon atoms in the undoped sample is also provided as shown in Fig. 3c. The predominant binding energy of the carbon atom in the undoped sample is around 284.6 eV, which is significantly different from that of TU-TiO_2 centered at 282.8 eV,

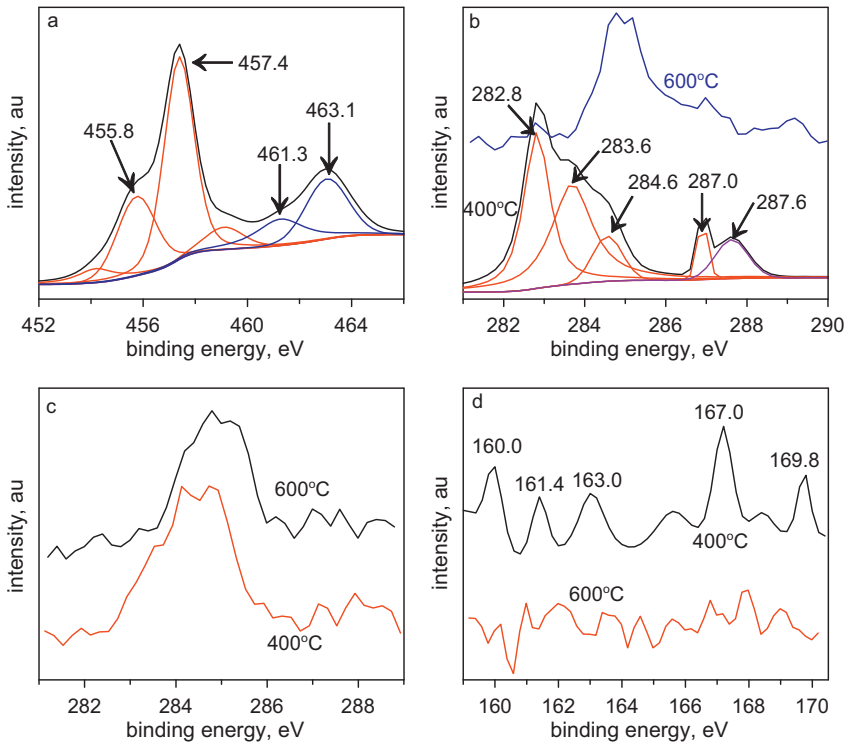

Fig. 3. XPS spectra displaying the (a) Ti 2p, (b) C 1s of the TU-14 sample, (c) C 1s of the undoped sample, and (d) S 2p regions of the TU-14 sample calcined at 400 and 600 °C.

indicating different distribution of carbon states existed between the undoped and TU-TiO_2 samples.

Fig. 3d presents the XPS spectrum of the S 2p region. At 400 °C, the maximum peak, located at 167.2 eV, can be assigned to S^{4+}, implying that S^{4+} centers can be incorporated into the TiO_2 bulk phase to substitute for Ti^{4+} ions. Furthermore, we also observed a band at 169.8 eV that we attribute to S^{6+} species. In addition to the cationic forms of S atoms, S^{2-} ions were also present, as indicated by the bands at 160.0 and 161.4 eV. However, the ionic radius of S^{2-} (0.17 nm) is significantly larger than that of O^{2-} (0.122 nm) and the bond energy of Ti–S (418.0 kJ/mol) is smaller than that of Ti–O (672.4 kJ/mol) [11,32,43]; as a result, the Ti–S bond is present at a lower level. However, the prepared procedure and precursors of sulfur atoms are also important factors affecting the chemical state [44]. When the calcined temperature increases to 600 °C, both the anionic and cationic S ions are almost completely eliminated from the sample.

Fig. 4 presents UV–vis diffuse reflectance spectra of the undoped, U-, T-, and TU-doped TiO_2 samples. The undoped TiO_2 sample displayed the strongest visible light absorbance, while the U-TiO_2 sample displayed visible light absorbance that was lower – albeit still significant – than those of the undoped, T-, and TU-TiO_2 samples. We suspect that the decreased photoabsorbance associated with the U-TiO_2 sample within the visible region may be ascribed to the decreased content of carbonaceous species and elemental carbons inherent from the precursors TTIP. Sulfur atoms from the precursor (thiourea) can substitute for both Ti and/or O atoms in the TiO_2 structure to form S-doped TiO_2, which can contribute to the visible light absorption as a result of band gap narrowing through the mixing of S 3p and O 2p electrons. This increased visible light absorbance after doping with S species cannot compensate, however, for the loss that resulted from the decreased C content. In addition, carbonaceous species and elemental carbons may exist in different structures for different samples and cause the deviation in visible light absorbance.

Fig. 5 displays the FTIR spectra of the undoped and doped TiO_2 samples after calcination at 400 °C. All the samples exhibit absorption signals at ca. 3425 and 1640 cm^{-1}, which we attribute to the stretching and bending vibrations, respectively, of the surface OH groups. We suspect that these OH bonds are connected to the bulk TiO_2 via both chemisorption and physisorption because we also observed IR absorptions at ca. 3000 cm^{-1} [8,43]. In addition, we found that a greater number of OH groups adsorbed onto the TiO_2 surfaces of the doped samples (particularly for the TiO_2 samples modified using thiourea as the precursor) than onto the undoped TiO_2 and commercial P-25 samples because the former samples exhibited stronger and broader IR absorption peaks corresponding to OH groups. As a result, we would expect these doped TiO_2 samples to possess higher photocatalytic activities because OH groups can be trapped by photogenerated holes to become OH free radicals. The U-TiO_2 sample absorbed significantly in the range from 950 to 1250 cm^{-1}. The bands centered at 1050, 1130, and 1220 cm^{-1}

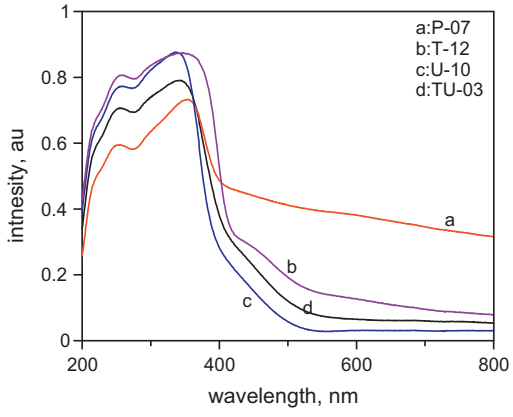

Fig. 4. UV–vis diffuse reflectance spectra of the P-07, T-12, U-10, and TU-03 samples calcined at 400 °C.

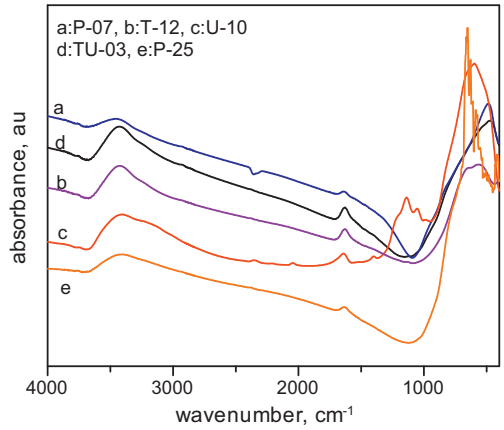

Fig. 5. FTIR spectra of the P-07, T-12, U-10, and TU-03 samples calcined at 400 °C.

Table 2
The measured specific surface areas and photocatalytic conversions of phenol, and the predicted ones from Eqs. (1) and (2), respectively.

Samples	Specific surface area, m^2/g		Conversion of phenol, %	
	Measured	Predicted	Measured	Predicted
TU-01	71.6	71.2	31.9	31.0
TU-02	110.5	106.8	22.1	22.1
TU-03	129.2	139.7	26.1	24.6
U-04	20.9	29.0	10.9	13.4
TU-05	143.9	139.7	24.2	24.6
T-06	60.8	56.4	18.6	19.8
P-07	19.4	18.9	5.9	5.7
TU-08	109.6	108.7	23.7	20.9
TU-09	144.5	139.7	23.8	24.6
U-10	44.1	49.4	27.9	28.9
TU-11	134.8	132.6	20.4	19.7
T-12	6.3	2.7	24.6	25.0
TU-13	135.0	139.7	22.1	24.6
TU-14	105.8	101.9	39.2	39.5
T-15	44.5	51.0	27.2	26.2
TU-16	120.3	117.4	29.3	26.9
TU-17	134.2	139.7	23.1	24.6
TU-18	125.3	118.8	27.4	28.5
TU-19	81.1	86.3	37.8	38.3
U-20	46.9	39.2	23.6	21.1

are indicative of C_{2v} symmetry, suggesting bidentate coordination between sulfate and TiO_2, while these at 987 and 1130 cm^{-1} can be ascribed to monodentate sulfate coordination, indicative of C_{3v} symmetry [45].

Table 2 lists the measured BET surface areas associated with the compositions of TTIP, $SnCl_4$ and thiourea. A simplified quartic model through a mixture design experiment and the commercial software Design Expert was developed to correlate the experiment and can be expressed in Eq. (1), with Y_1 representing the predicted

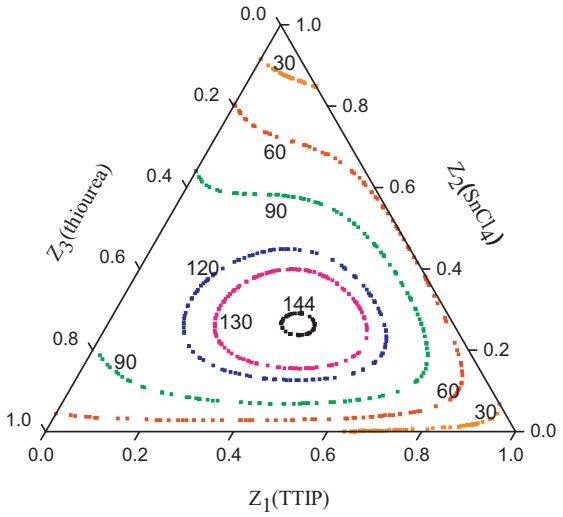

Fig. 6. Contours of constant specific surface area, obtained from Eq. (1).

surface area. The standard errors of the coefficients in Eq. (1) are presented in parentheses below the corresponding coefficients. We applied variance analysis to evaluate the adequacy of Eq. (1); Table 3 summarizes the results.

$$Y_1 = \underset{(5.45)}{18.87Z_1} + \underset{(6.32)}{2.72Z_2} + \underset{(5.45)}{49.41Z_3} + \underset{(28.52)}{192.95Z_1Z_2} + \underset{(28.52)}{306.19Z_2Z_3} + \underset{(525.5)}{4570.57Z_1{}^2Z_2Z_3} - \underset{(538.6)}{1364.53Z_1Z_2{}^2Z_3} + \underset{(526.6)}{1698.13Z_1Z_2Z_3{}^2} \quad (1)$$

The F test for the regression model, defined as the ratio of the mean square of the model to the residue, was 126.3; this value is greater than the tabled $F(p-1, \nu, \alpha)$ value of 4.64 at the α risk probability level of 0.01. The symbols p and ν represent the number of parameters in Eq. (1) and the degree of freedom of the residue, respectively. This result implies that this model is significant relative to the residue. Furthermore, the residue can be divided into residues of lack of fit and pure error, representing the inadequacy of the model form and experimental error, respectively. The corresponding F value of lack of fit to pure error was only 1.05, which is considerably lower than the tabled $F(8, 4, 0.01)$ value of 14.80 [24,25]. In addition, the correction coefficient (R^2) reached as high as 0.99, indicating that Eq. (1) describes the experimental data well. Furthermore, because the value of Pred. R^2 of 0.98 is in reasonable agreement with the Adj. R^2 of 0.94, Eq. (1) can be applied to predict future experimental data. The predicted surface areas were also present in Table 2, which were in good agreement with the measured ones. Fig. 6 illustrates the contour lines for the surface area against the compositions of TTIP, $SnCl_4$, and thiourea, exhibiting

Table 3
Variance analysis of the quartic form fit of Eq. (1).

Source	Sum of squares	DF[a]	Mean square	F-value	P value (prob > F)
Model	40133.8	7	5733.4	126.3	<0.0001
Linear mixture	1525.6	2	762.8	16.8	0.0003
Z_1Z_2	2078.3	1	2078.3	45.8	<0.0001
Z_2Z_3	5231.8	1	5231.8	115.2	<0.0001
$Z_1{}^2Z_2Z_3$	3433.9	1	3433.9	75.6	<0.0001
$Z_1Z_2{}^2Z_3$	291.4	1	291.4	6.4	0.0263
$Z_1Z_2Z_3{}^2$	472.1	1	472.1	10.4	0.0073
Residual	544.8	12	45.4		
Lack of fit	368.9	8	46.1	1.05	0.5182
Pure error	175.9	4	44.0		
Cor. total	40678.59	19			

[a] Degree of freedom.

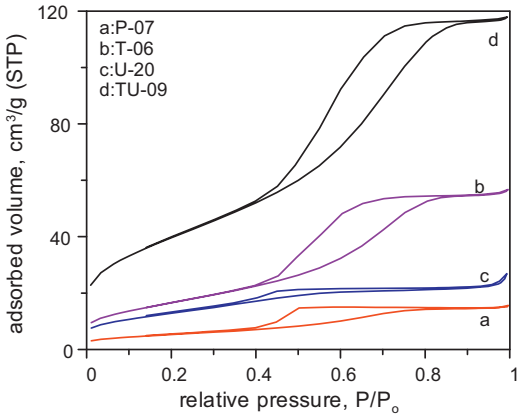

Fig. 7. N_2 adsorption/desorption isotherms of the 400 °C-calcined P-07, T-06, U-20, and TU-09 samples.

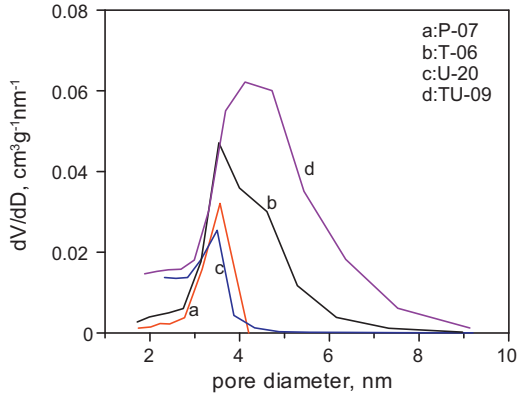

Fig. 8. BJH pore size distributions from desorption branches of the P-07, T-06, U-20, and TU-09 samples calcined at 400 °C.

the maximum surface area of 144.7 m^2/g at compositions (X_1, X_2, X_3) of (0.705, 0.135, 0.16).

Figs. 7 and 8 present the N_2 adsorption/desorption isotherms and BJH desorption pore size distribution curves, respectively, for the P-, T-, U-, and TU-TiO_2 samples calcined at 400 °C exhibiting the maximum specific surface areas (i.e., the samples P-07, T-06, U-20 and TU-09, respectively). Each of these prepared samples revealed a type IV isotherm with a H2 hysteresis loop in the approximate range $0.4 < P/P_o < 0.85$, which is characteristic of mesoporous structures formed through the agglomeration of nanoparticles having different particle sizes. The TU- and P-TiO_2 samples provided the highest and lowest specific adsorbed N_2 volumes, respectively, indicating that codoping with S and SnO_2 can feature TiO_2 samples with highly porous structure. The pore size distribution of the P–TiO_2 sample was similar to that of the U-sample, except that the latter revealed

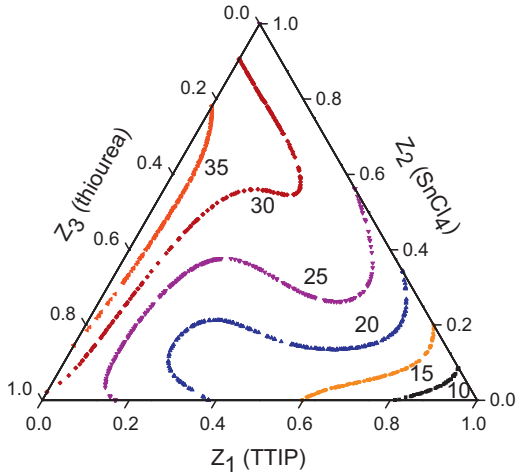

Fig. 9. Contours of constant conversion of phenol, obtained from Eq. (2).

a broader distribution of pore sizes. Doping with SnO_2 widened the pore size distribution of the sample; indeed, the sample codoped with S and SnO_2 exhibited the broadest pore size distribution. These results suggest that interactive effects exist between S, SnO_2 and TiO_2 that affect the morphology of the doped-TiO_2 samples and in turn the photocatalytic activity.

Table 2 provides the measured conversions of phenol with respect to the design compositions; we obtained maximum and minimum values of 39.2 and 5.9% at compositions (X_1, X_2, X_3) of (0.5, 0.167, 0.333) and (1.0, 0, 0), respectively. Following the regression analysis, a special quartic model, represented by Eq. (2) with Y_2 representing the conversion, was obtained. The predicted conversions were also listed in Table 2, which were reasonably consistent with the measured ones at corresponding compositions, indicating this model correlated the experiment data well. The variance analysis shown in Table 4 as well as the values of R^2, Pred. R^2, and Adj. R^2 of 0.96, 0.94, and 0.91, respectively, confirm the adequacy of this empirical model.

$$Y_2 = \underset{(1.46)}{5.65Z_1} + \underset{(1.70)}{25.01Z_2} + \underset{(1.46)}{28.88Z_3} - \underset{(7.53)}{34.44Z_1Z_2} + \underset{(7.53)}{53.77Z_2Z_3} + \underset{(130.2)}{446.8Z_1{}^2Z_2Z_3} - \underset{(130.3)}{859.5Z_1Z_2Z_3{}^2} \quad (2)$$

Fig. 9 displays the contour lines for the conversions of phenol with respect to the compositions of TTIP, $SnCl_4$, and thiourea, plotted using a response surface method. Although the undoped TiO_2 sample features the most visible light harvesting; however, both the experimental results and the empirical equation confirm that the undoped TiO_2 samples exhibited the poorest photocatalytic activity. It is suggested that the carbonaceous species adsorbed on the surface or located in the interstitial space of the undoped sam-

Table 4
Variance analysis of the quartic form fit of Eq. (2).

Source	Sum of squares	DF[a]	Mean square	*F*-value	*P* value (prob > *F*)
Model	1055.4	6	175.91	52.91	<0.0001
Linear mixture	762.6	2	381.30	114.69	<0.0001
Z_1Z_2	69.5	1	69.51	20.91	0.0005
Z_2Z_3	169.4	1	169.37	50.94	<0.0001
$Z_1{}^2Z_2Z_3$	39.1	1	39.13	11.77	0.0045
$Z_1Z_2Z_3{}^2$	144.6	1	144.64	43.51	<0.0001
Residual	43.2	13	3.32		
Lack of fit	34.4	9	3.82	1.735	0.3128
Pure error	8.8	4	2.20		
Cor. total	1098.7	19			

[a] Degree of freedom.

Table 5
Conversion ratio of phenol photocatalyzed by N, S or C doped TiO_2 samples under visible light.

Dopant	Irradiated wavelength, nm	Calcined temperature, °C	Reaction time, min	Conversion ratio[a]	Reference no.
S, C	>400	400	90	3.3	This work
SnO_2, S, C	>400	400	90	4.9	This work
N, S, C	>400	450	60	3.7	[10]
C	>400	350	60	3.2	[13]
S	>410	600	60	12.5	[14]
N, S	>420	450	120	20.0	[18]
C	>420	250[b]	120	5.0	[4]

[a] Defined as the ratio of phenol conversion catalyzed by doped TiO_2 to that by commercial P-25; roughly estimated from the data shown in figures in literature.
[b] Hydrothermal temperature.

ple can efficiently absorb the incident irradiation to excite electrons from the HOMO to LUMO state; however, these electrons fail to promote the degradation of phenol, which may be due to the fast recombination. Incorporating SnO_2 into TiO_2 increased the conversion from 5.9 to 27.2% as the SnO_2 fraction increased from 0 to 33.3%, but then it decreased to 24.6% as the fraction increased further to 50%. The dependence of the activity of the T-TiO_2 sample on the fraction of SnO_2 was similar to that of the surface area, i.e., the surface area affected the activity to some extent. In addition, SnO_2, possessing lower conduction band position and higher conductivity than those of TiO_2, can enhance the separation and transportation of the charge carriers, preventing the recombination of e^- and h^+ and elevating the photocatalytic efficiency [19,46,47]. We suggest that these factors together led to the increase in photocatalytic activity upon increasing the SnO_2 content. On the other hand, the use of excess SnO_2 decreased the crystallization of the TiO_2 and enhanced the recombination of photogenerated charged carriers [20], thereby decreasing its photocatalytic efficiency.

Incorporating S into TiO_2 monotonously increased the conversion from 5.9 to 27.9% as the thiourea faction increased from 0 to 50%. Sulfur atoms can substitute for Ti or O atoms in TiO_2 structures, thereby increasing the visible light-induced photocatalytic activity. In addition, thiourea modification leads to the formation of O–Ti–C bonds, which are accepted as the active species in raising visible light activity [48]. Therefore, the photocatalytic activity of the TU-TiO_2 sample was superior to those of the P-, T- and U-TiO_2 samples in average; however, some tertiary systems exhibited lower photocatalytic activity when compared with the binary systems, which indicated that the composition of the precursors is indeed a vital cause in determining the photocatalytic activity. The increase in the photogeneration of electrons and holes resulting from the incorporation of S and C atoms, and the increases in the separation and transport efficiencies of e^- and h^+ caused by SnO_2 modification are suggested to enhance the visible light-induced photocatalytic activity. The interaction among S, C, SnO_2, and TiO_2, causing the stabilization of anatase structure, the increase of specific surface area, and the change of morphology of TiO_2 samples, is also an important factor to enhance the photocatalytic activity. The derived empirical equation predicted that a maximum conversion of 40.4% would occur at a composition of (0.5, 0.23, 0.27); this value is very close to the measured conversion of 41.7%, confirming the adequacy of the quartic model.

Table 5 provides the conversion ratio, defined as the ratio of phenol conversion photocatalyzed by the doped TiO_2 sample to that by commercial P-25, in this work as well as those reported by other groups [4,10,13,14,18]. Although the calcined temperature was not optimized, our S, C-doped TiO_2 sample still showed a conversion ratio of 3.3, which was comparable to those of 3.7 and 3.2 in literature [10,13]. Incorporating appropriate SnO_2 to the S, C-doped TiO_2 increases the conversion ratio to 4.9, which is indicative of a synergic effect between SnO_2 and S, C dopants on the visible light activity of TiO_2. These results clearly imply that the mixture design approach is a facile and effective route to search for the optimal composition of the precursors of $SnCl_4$, thiourea, and TTIP to fabricate the S, C, and SnO_2-codoped TiO_2 photocatalyst exhibiting the optimal visible light activity.

4. Conclusion

A synergic effect between SnO_2 and S, C species on the visible light activity of TiO_2 was observed. Combining SnO_2 and S, C species can increase the pore size and the surface area of TiO_2, and increase the number of OH groups on the TiO_2 surface, which were beneficial to increase photocatalytic activity, when compared to doping with SnO_2 or S, C species alone. In addition, S, C species can effectively inhibit the anatase-to-rutile transformation of TiO_2, which was promoted by SnO_2, in addition to the origin of visible light activity. Using the mixture design experimental method, we successfully obtained quartic models that describes quite well the effects of the composition of the precursors – TTIP, tin chloride, and thiourea – on the visible light-induced activity and the specific surface area of the codoped TiO_2 samples. This model predicted that optimal mole fractions of (TTIP, tin chloride, thiourea) of (0.5, 0.23, 0.27) and (0.705, 0.135, 0.16) would provide a phenol conversion of 40.4% and a surface area of 144.7 m^2/g, which are in good agreement with the measured results of 41.7% and 141.9 m^2/g, respectively.

Acknowledgment

We thank the National Science Council of Taiwan, Republic of China, for supporting this study financially under contract NSC-95-2745-E-168-005-URD.

References

[1] C. Lettmann, K. Hildenbrand, H. Kisch, W. Macyk, W.F. Maier, Visible light photodegradation of 4-chlorophenol with a coke-containing titanium dioxide photocatalyst, Appl. Catal. B: Environ. 32 (2001) 215–227.
[2] L.C. Chen, C.M. Huang, F.R. Tsai, Characterization and photocatalytic activity of K^+-doped TiO_2 photocatalysts, J. Mol. Catal. A: Chem. 265 (2007) 133–140.
[3] O. Carp, C.L. Huisman, A. Reller, Photoinduced reactivity of titanium dioxide, Prog. Solid State Chem. 32 (2004) 33–177.
[4] H.J. Yun, H. Lee, J.B. Joo, N.D. Kim, M.Y. Kang, J. Yi, Facile preparation of high performance visible light sensitive photo-catalysts, Appl. Catal. B: Environ. 94 (2010) 241–247.
[5] C.D. Valentin, G. Pacchioni, A. Selloni, Theory of carbon doping of titanium dioxide, Chem. Mater. 17 (2005) 6656–6665.
[6] R. Asahi, T. Morikawa, T. Ohwaki, K. Aoki, Y. Taga, Visible-light photocatalysis in nitrogen-doped titanium oxides, Science 293 (2001) 269–271.
[7] S.U.M. Khan, M. Al-Shahry, W.B. Ingler Jr., Efficient photochemical water splitting by a chemically modified *n*-TiO_2, Science 297 (2002) 2243–2245.
[8] Y. Huang, W. Ho, S. Lee, L. Zhang, G. Li, J.C. Jimmy, Effect of carbon doping on the mesoporous structure of nanocrystalline titanium dioxide and its solar-light-driven photocatalytic degradation of NO*x*, Langmuir 24 (2008) 3510–3516.
[9] T. Ohno, M. Akiyoshi, T. Umebayasshi, K. Asai, T. Mitsui, M. Matsumura, Preparation of S-doped TiO_2 photocatalysts and their photocatalytic activities under visible light, Appl. Catal. A: Gen. 265 (2004) 115–121.
[10] A. Zaleska, P. Górska, J.W. Sobczak, J. Hupka, Thioacetamide and thiourea impact on visible light activity of TiO_2, Appl. Catal. B: Environ. 76 (2007) 1–8.
[11] J.C. Yu, W. Ho, J. Yu, H. Yip, P.K. Wong, J. Zhao, Efficient visible-light-induced photocatalytic disinfection on sulfur-doped nanocrystalline titania, Environ. Sci. Technol. 39 (2005) 1175–1179.

[12] T. Umebayashi, T. Yamaki, S. Tanaka, K. Asai, Visible light-induced degradation of methylene blue on S-doped TiO_2, Chem. Lett. 32 (2003) 330–331.
[13] P. Górska, A. Zaleska, E. Kowalska, T. Klimczuk, J.W. Sobczak, E. Skwarek, W. Janusz, J. Hupka, TiO_2 photoactivity in vis and UV light: the influence of calcination temperature and surface properties, Appl. Catal. B: Environ. 84 (2008) 440–447.
[14] S. Liu, X. Chen, A visible light response TiO_2 photocatalyst realized by cationic S-doping and its application for phenol degradation, J. Hazard. Mater. 152 (2008) 48–55.
[15] Y. Zhao, X. Qiu, C. Burda, The effects of sintering on the photocatalytic activity of N-doped TiO_2 nanoparticles, Chem. Mater. 20 (2008) 2629–2636.
[16] T. Umebayashi, T. Yamaki, S. Yamamoto, A. Miyashita, S. Tanaka, T. Sumita, K. Asai, Sulfur-doping of rutile–titanium dioxide by ion implantation: Photocurrent spectroscopy and first-principles band calculation studies, J. Appl. Phys. 93 (2003) 5156–5160.
[17] H. Li, X. Zhang, Y. Huo, J. Zhu, Supercritical preparation of a highly active S-doped TiO_2 photocatalyst for methylene blue mineralization, Environ. Sci. Technol. 41 (2007) 4410–4414.
[18] J.-H. Xu, J. Li, W.-L. Dai, Y. Cao, H. Li, K. Fan, Simple fabrication of twist-like helix N,S-codoped titania photocatalyst with visible-light response, Appl. Catal. B: Environ. 79 (2008) 72–80.
[19] K. Vinodgopal, P.V. Kamat, Enhanced rates of photocatalytic degradation of an azo dye using SnO_2/TiO_2 coupled semiconductor thin films, Environ. Sci. Technol. 29 (1995) 841–845.
[20] J. Liqiang, F. Honggang, W. Baiqi, W. Dejun, X. Baifu, L. Shudan, S. Jiazhong, Effect of Sn dopant on the photoinduced charge property and photocatalytic activity of TiO_2 nanoparticles, Appl. Catal. B: Environ. 62 (2006) 282–291.
[21] M.N. Chong, H.Y. Zhu, B. Jin, Response surface optimization of photocatalytic process for degradation of Congo red using H-titanate nanofiber catalyst, Chem. Eng. J. 156 (2010) 278–285.
[22] D. Vildozo, C. Ferronato, M. Sleiman, J.-M. Chovelon, Photocatalytic treatment of indoor air: optimization of 2-propanol removal using a response surface methodology (RSM), Appl. Catal. B: Environ. 94 (2010) 303–310.
[23] M.C. Yeber, C. Soto, R. Riveros, J. Navarrete, G. Vidal, Optimization by factorial design of copper (II) and toxicity removal using a photocatalytic process with TiO_2 as semiconductor, Chem. Eng. J. 152 (2009) 14–19.
[24] J.A. Cornell, Experiments with Mixtures: Design, Models and the Analysis of Mixture Data, third ed., Wiley, New York, 2001.
[25] D.C. Montgomery, Design and Analysis of Experiments, forth ed., Wiley, New York, 1997.
[26] L.C. Chen, Y.C. Ho, W.S. Guo, C.M. Huang, T.C. Pan, Enhanced visible light-induced photoelectrocatalytic degradation of phenol by carbon nanotube-doped TiO_2 electrodes, Electrochim. Acta 54 (2009) 3884–3891.
[27] L.C. Chen, Y.J. Tu, Y.S. Wang, R.S. Kan, C.M. Huang, Characterization and photoreactivity of N-, S-, and C-doped ZnO under UV and visible light illumination, J. Photochem. Photobiol. A: Chem. 199 (2008) 170–178.
[28] S. Chappel, S.-G. Chen, A. Zaban, TiO_2-coated nanoporous SnO_2 electrodes for dye-sensitized solar cells, Langmuir 18 (2002) 3336–3342.
[29] Z.M. Shi, L. Yan, L.N. Jin, X.M. Lu, G. Zhao, The phase transformation behaviors of Sn^{2+}-doped titania gels, J. Non-Cryst. E Solids 353 (2007) 2171–2178.
[30] K.-N.P. Kumar, D.J. Fray, J. Nair, F. Mizukami, T. Okubo, Enhanced anatase-to-rutile phase transformation without exaggerated particle growth in nanostructured titania–tin oxide composites, Scripta Mater. 57 (2007) 744–771.
[31] P. Periyat, D.E. McCormack, S.J. Hinder, S.C. Pillai, One-pot synthesis of anionic (nitrogen) and cationic (sulfuric) codoped high-temperature stable, visible light active, anatase photocatalysts, J. Phys. Chem. C 113 (2009) 3246–3253.
[32] P. Periyat, S.C. Pillai, D.E. McCormack, J. Colreavy, S.J. Hinder, Improved high-temperature stability and sun-light-driven photocatalytic activity of sulfuric-doped anatase TiO_2, J. Phys. Chem. C 112 (2008) 7644–7652.
[33] S.C. Pillai, P. Periyat, R. George, D.E. McCormack, M.K. Seery, H. Hayden, J. Colreavy, D. Corr, S.J. Hinder, Synthesis of high-temperature stable anatase TiO_2 photocatalyst, J. Phys. Chem. C 111 (2007) 1605–1611.
[34] P. Cheng, J. Qiu, M. Gu, Y. Jin, W. Shangguan, Synthesis of shape-controlled titania particles from a precursor solution containing urea, Mater. Lett. 58 (2004) 3751–3755.
[35] B.X. Huang, P. Tornatore, Y.-S. Li, IR and Raman spectroelectrochemical studies of corrosion films on tin, Electrochim. Acta 46 (2000) 671–679.
[36] G. An, W. Ma, Z. Sun, Z. Liu, B. Han, S. Miao, Z. Miao, K. Ding, Preparation of titania/carbon nanotube composites using supercritical ethanol and their photocatalytic activity for phenol degradation under visible light irradiation, Carbon 45 (2007) 1795–1801.
[37] H. Liu, W. Yang, Y. Ma, J. Yao, Extended visible light response of binary TiO_2–Ti_2O_3 photocatalyst prepared by a photo-assisted sol–gel method, Appl. Catal. A: Gen. 299 (2006) 218–223.
[38] G. Colon, M.C. Hidalgo, G. Munurea, I. Ferino, M.G. Cutrufello, J.A. Navio, Structural and surface approach to the enhanced photocatalytic activity of sulfated TiO_2 photocatalyst, Appl. Catal. B: Environ. 63 (2006) 45–59.
[39] W. Ren, Z. Ai, F. Jia, L. Zhang, X. Fan, Z. Zou, Low temperature preparation and visible light photocatalytic activity of mesoporous carbon-doped crystalline TiO_2, Appl. Catal. B: Environ. 69 (2007) 138–144.
[40] C. Chen, M. Long, H. Zeng, W. Cai, B. Zhou, J. Zhang, Y. Wu, D. Ding, D. Wu, Preparation, characterization and visible-light activity of carbon modified TiO_2 with two kinds of carbonaceous species, J. Mol. Catal. A: Chem. 314 (2009) 35–41.
[41] M. Shen, Z. Wu, H. Huang, Y. Du, Z. Zou, P. Yang, Carbon-doped anatase TiO_2 obtained from TiC for photocatalysis under visible light irradiation, Mater. Lett. 60 (2006) 693–697.
[42] Z.M. Shi, X.Y. Ye, K.M. Liang, S.R. Gu, F. Pan, XPS analysis of light elements (C, N) remaining in sol–gel derived TiO_2 films, J. Mater. Sci. 22 (2003) 1255–1258.
[43] G. Li, L. Li, J. Boerio-Goates, B.F. Woodfield, High purity anatase TiO_2 nanocrystals: near room-temperature synthesis, grain growth kinetics, and surface hydration chemistry, J. Am. Chem. Soc. 127 (2005) 8659–8666.
[44] W. Ho, J.C. Yu, S. Lee, Low-temperature hydrothermal synthesis of S-doped TiO_2 with visible light photocatalytic activity, J. Solid State Chem. 179 (2006) 1171–1176.
[45] S.J. Hug, Insitu Fourier transform infrared measurements of sulfate adsorption on hematite in aqueous solutions, J. Colloid Interface Sci. 188 (1997) 415–422.
[46] Y. Cao, X. Zhang, W. Yang, H. Du, Y. Bai, T. Li, J. Yao, A bicomponent TiO_2/SnO_2 particulate film for photocatalysis, Chem. Mater. 12 (2000) 3445–3448.
[47] M. Zhou, J. Yu, S. Liu, P. Zhai, L. Jiang, Effects of calcination temperatures on photocatalytic activity of SnO_2/TiO_2 composite films prepared by an EPD method, J. Hazard. Mater. 154 (2008) 1141–1148.
[48] H. Kamisaka, T. Adachi, K. Yamashita, Theoretical study of the structure and optical properties of carbon-doped rutile and anatase titanium oxides, J. Chem. Phys. 123 (2005) 084704.